DESIGN OF ULTRA-HIGH TEMPERATURE CERAMICS FOR OXIDATION RESISTANCE

Rahim Zaman, Bi-Cheng Zhou (Advisor)

University of Virginia, Department of Materials Science and Engineering, Charlottesville, VA

April 13, 2023

Abstract

Phase relations in the HfO_2-Ta_2O_5 isopleth of the Hf-Ta-O system are investigated for the optimization of oxidation resistance in HfC-TaC alloys. Thermodynamic models of the Ta-O system and preliminary ones of the HfO_2-Ta_2O_5 system are developed using the CALculation of PHAse Diagrams (CALPHAD) method. The calculated phase diagram of the Ta-O system including the body-centered cubic (BCC) Ta, orthorhombic (O) and tetragonal (T) Ta_2O_5 polymorphs, ionic liquid, and gas phases, is consistent with prior experimental phase diagrams. In addition, first-principles calculations of the mixing enthalpies of oxygen in BCC Ta and the formation enthalpies of O-Ta_2O_5 agree with the current models and prior experimental data. The preliminary HfO_2-Ta_2O_5 phase diagram agrees with experimental data from the literature and can be used to evaluate the thermodynamic stability of the oxidation resistant $Hf_{(n-5)/2}Ta_2O_n$ ternary oxide series. Improved understanding of the thermal and oxidation resistance of HfC-TaC alloys will provide considerable benefits to aerospace and space exploration initiatives.

1. Introduction

Ultra-high temperature ceramics (UHTCs) have the highest attainable melting temperatures of greater than 3000 °C and favorable mechanical stabilities above 1650 °C. Due to their thermal resistance, UHTCs have been identified as potential materials for aerospace applications by the National Aeronautics and Space Administration (NASA) [1-3]. Hafnium carbide (HfC) and tantalum carbide (TaC), or (Hf,Ta)C, are UHTCs with the highest achievable melting temperatures of 3900 °C and 3880 °C, respectively [4]. Despite their high thermal stabilities, (Hf,Ta)C form oxidation products (HfO_2 and Ta_2O_5) with poor oxidation resistances and undergo severe oxidation within minutes of oxygen exposure above 1600 °C, which limits their use. Nevertheless, the composition of HfC-TaC alloys can be controlled to thermally grow protective oxide layers to lessen substrate degradation. HfC-TaC alloys have been found to form a ternary oxide ($Hf_6Ta_2O_{17}$) with an improved oxidation resistance compared to those of HfO_2 and Ta_2O_5 [5]. $Hf_6Ta_2O_{17}$ is in a homologous series ($Hf_{(n-5)/2}Ta_2O_n$), in which n ranges from 13 to 21 [6]. The high thermochemical stability of $Hf_6Ta_2O_{17}$ is desirable in high-temperature applications, including thermal protection systems, propulsion systems, and hypersonic aircraft design. However, the phase equilibria of the HfO_2-Ta_2O_5 isopleth in the Hf-Ta-O system, including the stabilities of $Hf_6Ta_2O_{17}$ and $Hf_{(n-5)/2}Ta_2O_n$, remain disputed. CALculation of PHAse Diagrams (CALPHAD) models [7] of the Ta-O system, described in detail by Meisner *et al.* [8], and preliminary ones of the Hf-Ta-O and HfO_2-Ta_2O_5 systems, which will be described in detail by Zaman and Zhou [9], were developed in the present study to describe the ternary system and gain better understanding of its phase relations. The models combine experimental data with calculated thermochemical properties to obtain optimized phase diagrams.

2. Review of Prior Data

2.1. Phases and Phase Transformations in the Hf-Ta-O System

The equilibrium, ambient pressure Hf-Ta-O system consists of hexagonal close-packed (HCP) α-Hf, body-centered cubic (BCC) β-Hf, BCC Ta, three polymorphs of HfO_2 (monoclinic (M), tetragonal (T), and cubic (C)), two polymorphs of Ta_2O_5 (low-temperature orthorhombic (O) and high-temperature tetragonal (T)), an orthorhombic $Hf_{(n-5)/2}Ta_2O_n$ series [10, 11], liquid phase, and gas phase. The crystal structures of the solid phases and phase transformations considered in the present study are respectively summarized in Tables 1 and 2.

Table 1. Ambient pressure crystal structures of condensed phases in the Hf-Ta-O system determined using X-ray diffraction (XRD), X-ray powder diffraction (XRPD), electron microscopy (EM), selected area electron diffraction (SAED), and neutron diffraction (ND).

Phase	Crystal Structure (SG = Space Group)	Lattice Parameters (Å)	Technique	Reference
α-Hf	HCP ($P6_3/mmc$, SG 194)	a = 3.198, c = 5.061	XRD	[12]
β-Hf	BCC ($Im\bar{3}m$, SG 229)	a = 3.615	XRD	[12]
Ta	BCC ($Im\bar{3}m$, SG 229)	a = 3.303	Single-Crystal XRD	[13]
M-HfO_2	Monoclinic ($P2_1/c$, SG 14)	a = 5.114, b = 5.168, c = 5.290, β = 99.211°	XRD	[14]
T-HfO_2	Tetragonal ($P4_2/nmc$, SG 137)	a = 3.645, c = 5.327	XRD	[15]
C-HfO_2	FCC ($Fm\bar{3}m$, SG 225)	a = 5.250	XRD	[15]
O-Ta_2O_5	Orthorhombic ($Pmm2$, SG 25)	a = 43.998, b = 3.894, c = 6.209	XRPD	[16]
T-Ta_2O_5	Tetragonal ($I4_1/amd$, SG 141)	a = 3.86, c = 36.18	EM, SAED	[17]
O-$Hf_4Ta_2O_{13}$	Orthorhombic ($Ima2$, SG 46)	a = 30.623, b = 4.943, c = 5.264	Removal of seven-coordinated polyhedra from O-$Hf_6Ta_2O_{17}$	[6]
O-$Hf_6Ta_2O_{17}$	Orthorhombic ($Ima2$, SG 46)	a = 40.831, b = 4.943, c = 5.264	XRPD, ND	[6]
O-$Hf_8Ta_2O_{21}$	Orthorhombic ($Ima2$, SG 46)	a = 51.038, b = 4.943, c = 5.264	Addition of seven-coordinated polyhedra to O-$Hf_6Ta_2O_{17}$	[6]

Table 2. Ambient pressure phase transformations in the Hf-Ta-O system.

Phase Transformation	Temperature (K)	Technique	Reference
α-Hf → β-Hf	2050	XRD, Optical Pyrometry	[12]
β-Hf → Liquid	2503	Oscilloscopy	[18]
Ta → Liquid	3290	Optical Pyrometry	[19]
M-HfO_2 → T-HfO_2	1988	XRPD, Single-Band Pyrometry, Spectropyrometry	[11]
T-HfO_2 → C-HfO_2	2873	XRPD, Single-Band Pyrometry, Spectropyrometry	[11]
C-HfO_2 → Liquid	3023	Thermal Arrest Experiments	[11]
O-Ta_2O_5 → T-Ta_2O_5	1633	XRPD, Single-Band Pyrometry, Spectropyrometry	[11]
T-Ta_2O_5 → Liquid	2133	Thermal Arrest Experiments	[11]
T-Ta_2O_5 + Liquid 1 → Liquid 2	2097	Thermal Arrest Experiments	[11]
O-$Hf_6Ta_2O_{17}$ → T-HfO_2 + Liquid	2517	Thermal Arrest Experiments	[11]
O-Ta_2O_5 + O-$Hf_6Ta_2O_{17}$ → T-Ta_2O_5	1573	Thermal Arrest Experiments	[11]
T-Ta_2O_5 + O-$Hf_6Ta_2O_{17}$ → Liquid	2004	Thermal Arrest Experiments	[11]

2.2. Ta-O Binary Subsystem

2.2.1. Proposed Crystal Structures of O-Ta_2O_5

A number of crystal structures have been proposed for O-Ta_2O_5, commonly referred to as β-Ta_2O_5, at ambient pressure using XRPD and XRD, as well as density functional theory (DFT), but the exact structure remains under debate. The predicted structures as of yet are summarized in Table 3. β-Ta_2O_5 is generally accepted to be orthorhombic, but monoclinic, tetragonal, and hexagonal structures have also been proposed. Nevertheless, the experimental nonstoichiometric $Ta_{24}O_{62}$

structure with partial occupation of oxygen sites predicted by Hummel *et al.* [16] was assumed for the present study due to the similarity of its lattice parameters and coordination environments to those of the α polymorph. The latter was previously refined to be a tetragonal $I4_1/amd$ structure with lattice parameters a = 3.86 Å and c = 36.18 Å using high-resolution EM and SAED techniques [17]. Furthermore, multiple metastable oxides have been reported in the Ta-O system [20], but were not considered in the present models.

Table 3. Proposed crystal structures of β-Ta_2O_5.

Structure	Technique	a	b	c	Reference
β (*$P2_12_12$*)	XRPD	6.18	43.93	3.89	[21]
β (*C2mm*)	XRPD	6.20	3.66	3.89	[22]
δ (*P6/mmm*)	XRPD	7.25	7.25	3.88	[23, 24]
β (*Pna2*)	XRPD	14.65	9.40	31.19	[25]
L (*P2mm*)	XRPD	6.20	40.29	3.89	[26]
T (*Pmm2*)	XRPD	44.00	3.89	6.21	[16]
B (*C2/c*)	XRPD	12.79	4.85	5.53	[27]
β (*Pccm*)	XRPD	6.22	3.68	7.79	[28]
L (*C112/m*)	XRD	6.19	69.55	3.89	[29]
δ (*P6/mmm*)	DFT	7.19	7.19	3.83	[24]
Pm	DFT	6.30	3.79	11.14	[30, 31]
β (*Pmma*)	DFT	7.13	6.03	3.82	[32]
λ (*Pbam*)	DFT	6.25	7.40	3.83	[33]
***Pmmn* (mp-1539317)**	DFT	3.87	3.90	13.13	[34]
Cmmm	DFT	3.81	12.79	3.79	[35]
γ (*$I4_1/amd$*)	DFT	3.88	3.88	26.27	[31]

2.2.2. Oxygen Solubility in BCC Ta

BCC Ta has been determined to have oxygen solubility up to 6.39 at% using oxygen absorption [36], vacuum fusion analysis [37] and electrochemical methods [38, 39]. Oxygen partial pressures (P_{O_2}) as functions of the atomic ratio of oxygen to tantalum and temperature were determined [40] using prior solubility measurements from an electrochemical ThO_2-Y_2O_3 cell [41]. Since the current study described the Ta-O system at atmospheric pressure, the prior experimental P_{O_2} in BCC Ta were treated as oxygen activities and inputted into the CALPHAD models.

2.2.3. Prior Thermodynamic Data of Ta_2O_5

A review of the thermodynamic data of both Ta_2O_5 polymorphs has been published by Jacob *et al.* [42]. They tabulated the enthalpies, heat capacities, entropies, and Gibbs energies of formation using electrochemical measurements and prior data from the literature with additional corrections to account for the solubility of oxygen in tantalum electrodes. Since the thermochemical properties tabulated by Jacob *et al.* are the most comprehensive ones and their study assumed an O-Ta_2O_5 structure with a coordination similar to that of Hummel *et al.*, their data was used as inputs for the current CALPHAD models.

2.2.4. Prior Studies of the Ta-O Phase Diagram

The complete Ta-O phase diagram was first experimentally studied by Jehn and Olzi [37] using microscopy of quenched Ta-O samples and vacuum fusion analysis of oxygen-saturated Ta. They determined that the liquid phase has a miscibility gap, as well as eutectic and monotectic invariant equilibria. While Jehn and Olzi qualitatively estimated the liquidus curve based on the quantitative invariant equilibria, the liquidus has no phase data and results in an unrealistic α-Ta_2O_5 + Liquid phase. Consequently, only the condensed and invariant liquid phase equilibria were used as inputs into the current models, while the liquid parameters were qualitatively modified to agree with the preliminary experimental liquidus. In regard to prior thermodynamic modeling, an evaluation of the system was performed [40] but is incompatible and cannot be extended to higher order systems with the CALPHAD methodology. The present study modeled the Ta-O system with the CALPHAD approach using prior experimental data from the literature, supplemented by first-principles calculations.

2.3. Hf-O Binary Subsystem

The Hf-O phase diagram has been previously modeled by Shin [43, 44] and Wang [45] using the CALPHAD method. However, their models can be further optimized to better fit prior experimental data. This optimization will be discussed in a future publication by the authors [9].

2.4. Hf-Ta Binary Subsystem

The Hf-Ta system was assessed by Guillermet [46] using the CALPHAD method. The calculated phase diagram is consistent with prior experimental data and the binary interaction parameters were adopted in the present models.

2.5. HfO_2-Ta_2O_5 Isopleth

A comprehensive phase diagram of the HfO_2-Ta_2O_5 isopleth in the Hf-Ta-O system was experimentally determined by McCormack *et al.* [11] using thermal arrest and in-situ XRPD experiments, and was later revised based on comments from Fedorov [47]. Phase data points from McCormack *et al.* and additional liquidus data from a preliminary HfO_2-Ta_2O_5 phase diagram by Turcotte [48] were used as inputs for the current optimization, and phase boundaries from the former were used to qualitatively adjust the model parameters. The phase transformations and temperatures obtained by McCormack *et al.* are shown in Table 2.

3. Methods

3.1. First-Principles Calculations

3.1.1. Ta-O Subsystem

The 0-K formation enthalpies of the T (*pmm2*) and *Pmmn* structures of O-Ta_2O_5, as well as the enthalpies of mixing of oxygen in BCC Ta, were calculated using DFT and compared to the modeled values. The *Pmmn* structure was considered since it is the most stable one in the Materials Project Database [34]. Crystal structures of O-Ta_2O_5 and BCC Ta listed in Table 1 were used as input structures for the DFT calculations, all of which were performed in the Vienna Ab initio Simulation Package (VASP). The local density approximation (LDA) [49] was used to account for strong interactions between metal and oxygen atoms. As is common for metal-oxygen systems, an energy cutoff of 520 eV was used to model interactions between ions and electrons with the projector augmented wave (PAW) method. To optimize computational accuracy, gamma-centered k-point meshes with approximately 10,000 k-points and the tetrahedron method with Blöchl corrections were used for all calculations. Valence states of 5p6s6d and s^2p^4 were used for Ta and O, respectively.

The 0-K enthalpies of formation (ΔH_f) of O-Ta_2O_5 were computed from the elemental reference states using Equation 1, in which E_0 is the total energy of the respective fully relaxed structure from DFT. The resulting 0-K ΔH_f of both forms of O-Ta_2O_5 were compared with each other and with the modeled values at 298 K using a convex hull.

$$\Delta H_{f,0-K}^{O-Ta_2O_5} = E_0(O-Ta_2O_5) - 2E_0(Ta) - \frac{5}{2}E_0(O_2) \quad (1)$$

The total energy of spin-polarized O_2 was calculated based on an isolated molecule in a 10 x 10 x 10 Å cubic cell, which is in contrast to the non-spin-polarized calculation used in the original modeling of the Ta-O system by the authors [8].

Oxygen solubility in BCC Ta was modeled by mixing enthalpies calculated using special quasi-random structures (SQS). SQS were generated using the corrdump and mcsqs codes in the Alloy Theoretic Automated Toolkit (ATAT) [50], and assumed that oxygen primarily dissolves in BCC octahedral interstitial sites. Octahedral occupancies between 1/18 and 2/3, representing oxygen mole fractions between 0.04 and 0.50, were used to generate 48-atom SQS. The resulting mixing enthalpy as a function of oxygen mole fraction was calculated using Equation 2:

$$\Delta H_{mix}^{Ta_{12}O_nVa_{36-n}} = E_0(Ta_{12}O_nVa_{36-n}) - 12E_0(Ta) - \frac{n}{2}E_0(O_2) \quad (2)$$

where n includes integers between 2 and 24. Because $E_0(Ta_{12}O_nVa_{36-n})$ was modeled using SQS, mechanical instabilities were considered through use of the recently developed inflection-detection method, implemented in VASP by the robustrelax code [51]. In addition to the SQS mixing enthalpies, the dilute mixing enthalpy of a single oxygen atom in a 27-atom BCC Ta supercell was calculated using Equation 3. The total energy of the dilute structure was obtained from a static DFT calculation.

$$\Delta H_{mix,dilute}^{Ta_{26}O_1} = E_0(Ta_{26}O_1) - 26E_0(Ta) - \frac{1}{2}E_0(O_2) \quad (3)$$

3.1.2. Hf-Ta-O System

DFT and quasiharmonic phonon calculations were performed to respectively obtain 0-K and finite temperature properties of M-HfO_2, O-Ta_2O_5, and O-$Hf_6Ta_2O_{17}$ as inputs for the CALPHAD models. Calculated properties included enthalpies of formation of each oxide, entropies, Gibbs energies, and heat capacities of M-HfO_2 and O-$Hf_6Ta_2O_{17}$, and mixing enthalpies of Hf and Ta in O-Ta_2O_5 and O-$Hf_6Ta_2O_{17}$. Additional thermochemical data was calculated and compared to prior experimental data to verify the accuracy of the computations. These calculations will be discussed in detail in a future publication by the authors [9].

3.2. Thermodynamic Models

The compound energy formalism (CEF) [52-54] was used to model all phases in the Hf-Ta-O system. The CEF describes the total Gibbs energy of a phase based on a sublattice model and a constituent matrix (I), the latter of which describes sublattice site occupancies by constituents with site occupation fractions of y_i. In the CEF, a sublattice is a set of equivalent atomic positions in a crystal structure. The general form of the Gibbs energy of a phase according to the CEF is shown in Equations 4-7 [52, 54]:

$$G_m = {}^{srf}G_m + {}^{phys}G_m - T\,{}^{conf}S_m + {}^{E}G_m \quad (4)$$

$${}^{srf}G_m = \sum_{I_0} P_{I_0}(Y)\,{}^{o}G_{I_0} \quad (5)$$

$${}^{conf}S_m = -R\sum_{s=1}^{n} a_s \sum_{i=1}^{n_s} y_i^{(s)} \ln\left(y_i^{(s)}\right) \quad (6)$$

$${}^{E}G_m = \sum_{I_1} P_{I_1}(Y) L_{I_1} + \sum_{I_2} P_{I_2}(Y) L_{I_2} + \cdots \quad (7)$$

where G_m is the total molar free energy of a phase at temperature T, ${}^{srf}G_m$ is the Gibbs energy of the surface of reference, ${}^{phys}G_m$ is the physical Gibbs energy, ${}^{conf}S_m$ is the configurational entropy, and ${}^{E}G_m$ is the excess Gibbs energy. ${}^{srf}G_m$ represents the weighted average of the Gibbs energies of the constituents in a phase relative to their reference states, and depends on the product of the constituent fractions specified by I_0, $P_{I_0}(Y)$ and Gibbs energy of formation of compound I_0, ${}^{o}G_{I_0}$. ${}^{phys}G_m$ is the contribution of physical effects, primarily magnetism, to the Gibbs energy. In the equation for ${}^{conf}S_m$, R is the gas constant and a_s is the number of sites on each sublattice. ${}^{E}G_m$ includes contributions from the interactions between constituents, which are described by interaction parameters (L_I) and constituent fraction products of first and higher order I matrices $\left(P_I(Y)\right)$. Binary interaction parameters for ${}^{E}G_m$ can be described by a Redlich-Kister series [55], shown in Equation 8. The vth order ${}^{v}L_{ij}$ can be written in a two-parameter form, as in Equation 9, to include temperature dependence, where ${}^{v}a_{ij}$ and ${}^{v}b_{ij}$ are parameters to be optimized. Initially, zero- and first-order interaction parameters were used, but higher order ones were included as needed to obtain a better fit with the experimental phase data. Pure element reference state data was obtained from the SGTE database [56]. All parameters were optimized using the Thermo-Calc software [57].

$$L_{ij} = {}^{v}L_{ij}\sum_{v=0}^{n}\left(y_i - y_j\right)^{v} \quad (8)$$

$${}^{v}L_{ij} = {}^{v}a_{ij} + {}^{v}b_{ij}\cdot T \quad (9)$$

3.2.1. Ta-O Subsystem

The BCC Ta phase was modeled as a solid solution due to its significant oxygen solubility. The sublattice model $(Ta)_1(O,Va)_1$ was used to describe the phase based on the limited occupancies of octahedral interstitial sites in the BCC lattice by oxygen atoms [58]. A zero-order interaction parameter was sufficient to model the BCC Ta phase. O- and T-Ta_2O_5 were modeled as stoichiometric compounds with the two-sublattice model $(Ta)_2(O)_5$ based on the assumption that vacancy concentrations are negligible.

The liquid phase was modeled by the ionic two-sublattice model developed by Hillert *et al.* [59], which assumes random mixing of cations and anions on separate sublattices. The general model is $\left(C_i^{v_i^+}\right)_P\left(A_j^{v_j^-}, Va, B_k^0\right)_Q$, where $C_i^{v_i^+}$ represents cations of element i with a valence of v_i^+, $A_j^{v_j^-}$ anions of element j with a valence of v_j^-, Va hypothetical vacancies needed to maintain electroneutrality, and B_k^0 neutral components. The number of sites on each sublattice, P and Q, are

given by Equations 10 and 11, respectively, and the resulting simplified liquid phase model is $(Ta^{+5})_{2y_{O^{-2}}+5y_{Va^{-5}}}(O^{-2}, Va^{-5})_5$.

$$P = \sum_j \left(-v_j y_{A_j}\right) + Q y_{Va} \quad (10)$$

$$Q = \sum_i v_i y_{C_i} \quad (11)$$

3.2.2. Hf-Ta-O System

Modeled phases in the Hf-Ta-O system include those from the binary subsystems described in the previous sections, O- and T-Ta_2O_5, $Hf_4Ta_2O_{13}$, $Hf_6Ta_2O_{17}$, $Hf_8Ta_2O_{21}$, and a liquid phase. The homologous series of both Ta_2O_5 polymorphs [11, 48] were described as ionic solid solutions. The homologous series of ternary oxide phases [10, 11] was modeled as separate solid solutions with cation disorder. The liquid phase was described by the ionic two-sublattice model [59]. Details about the ternary modeling will be included in a separate publication [9].

4. Results and Discussion

4.1. Ta-O Subsystem

4.1.1. First-Principles Calculations

Lattice parameters of a = 43.37 Å, b = 3.82 Å, and c = 6.28 Å were obtained after full DFT relaxation of the T form of O-Ta_2O_5, which agree with the experimental values of a = 44.00 Å, b = 3.89 Å, and c = 6.21 Å [16]. The calculated parameters of the *Pmmn* form were a = 3.82 Å, b = 3.85 Å, and c = 12.94 Å, which are consistent with the initial values listed in Table 3. The calculated 0-K enthalpies of formation of -2047.38 kJ/mol and -2158.21 kJ/mol for the T and *Pmmn* forms, respectively, are 0.46% and 5.90% lower than the value of -2038.03 kJ/mol obtained by Jacob *et al.* [42] at 298 K using electrochemical measurements. The calculated values of the T and *Pmmn* structures are respectively 5.58% and 2.78% higher than the modeled values of -2168.34 kJ/mol and -2219.97 kJ/mol at the compositions $Ta_{24}O_{62}$ and Ta_2O_5 at 298 K, which is a favorable agreement. The comparison between 0-K DFT and CALPHAD model formation enthalpies is shown in the convex hull in Fig. 1. Unlike in the original modeling [8], the DFT enthalpies of formation are higher than the convex hull, but also closer in magnitude to the latter due to inclusion of spin-polarization in the calculation of the total energy of oxygen gas.

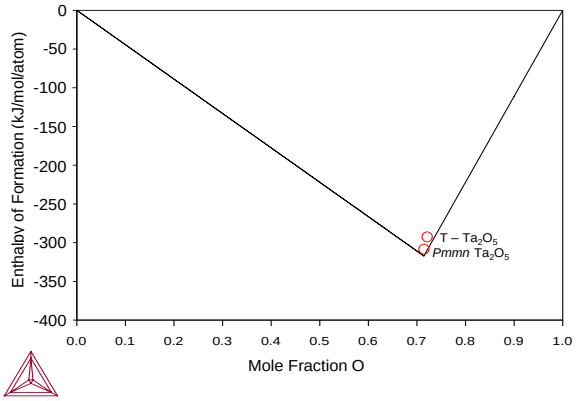

Fig. 1. Modeled convex hull of the tantalum-oxygen system at 298 K with the 0-K DFT enthalpies of formation of the T and *Pmmn* forms of O-Ta_2O_5 superimposed.

The calculated mixing enthalpies of oxygen in BCC Ta from DFT and the CALPHAD models are plotted as functions of oxygen mole fraction in Fig. 2. Favorable mixing is expected since the mixing enthalpies are negative and is consistent with the high oxygen solubility limit of the BCC phase in the Ta-O phase diagram. At low oxygen concentrations, the DFT mixing enthalpies agree well with those from the CALPHAD models, but at higher concentrations, the modeled values are significantly more negative than those from DFT. This difference is due to symmetry breaking of the SQS during full relaxation in the inflection-detection method caused by long-range interactions between electrons.

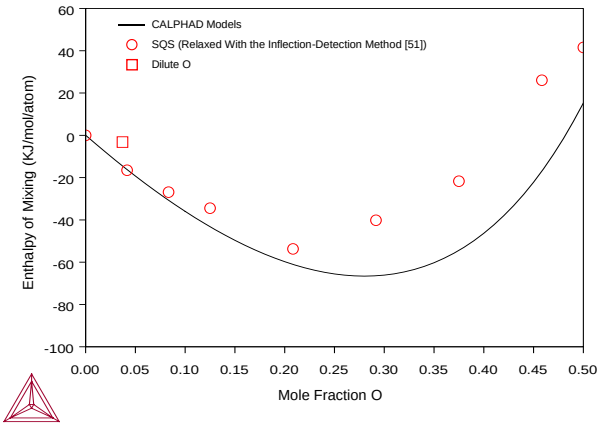

Fig. 2. Modeled enthalpies of mixing of oxygen in BCC Ta (solid curve) compared to those from SQS relaxations (open circles) and the dilute mixing enthalpy of one oxygen atom in a Ta matrix (open square).

4.1.2. CALPHAD Models

The calculated phase diagram of the Ta-O system is shown in Fig. 3, and the experimental solid-state and solvus data is well fit. Moreover, as shown in Figs. 4 and 5, the modeled heat capacities and entropies of both Ta_2O_5 polymorphs agree very well with values tabulated by Jacob *et al.* [42].

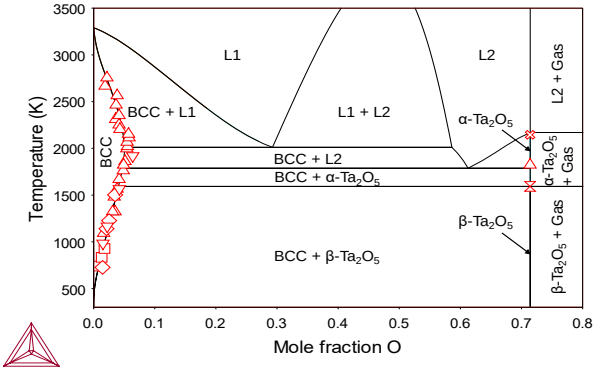

Fig. 3. Calculated phase diagram of the Ta-O system between 300 and 3500 K. Experimental data from [36-39, 60, 61].

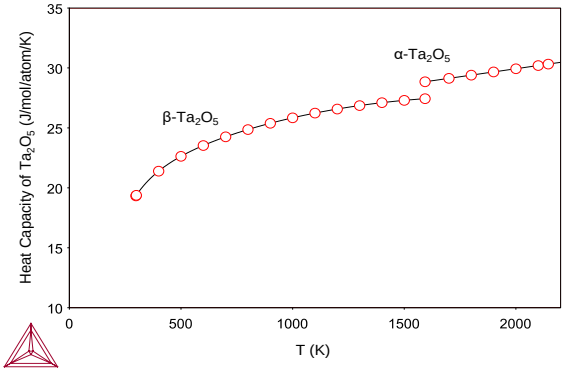

Fig. 4. Modeled heat capacities of α- and β-Ta_2O_5 (solid curves) compared with tabulated data [42].

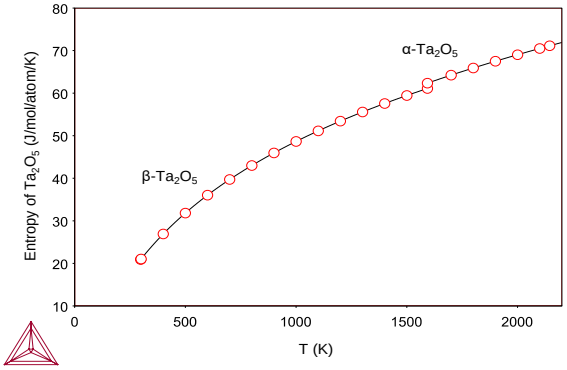

Fig. 5. Modeled entropies of α- and β-Ta_2O_5 (solid curves) compared with tabulated data [42].

The CALPHAD models predict favorable solubility and decrease in entropy associated with oxygen dissolution in BCC Ta, as $\Delta G^o = -439{,}246 + 69.987T$ J/mol. However, an accuracy trade-off was found between the fitting of the experimental BCC Ta solidus, and the monotectic and eutectic data. Since there is significantly more experimental solidus than liquidus data [37] available, the former was prioritized. Consequently, the monotectic and eutectic were respectively underestimated at 29.26 mol% O and 2011 K, and 61.27 mol% O and 1788 K compared to the experimental ones at 43 mol% O and 2153 K, and 71 mol% O and 1823 K [37]. Additional liquidus data would be necessary to improve the liquid phase fitting, but is difficult to obtain due to the miscibility gap and high temperatures involved. Nevertheless, the ionic liquid model provides a physically realistic description of the favorable ionization tendency of Ta to Ta^{+5} and O to O^{-2} in the liquid phase, and can be efficiently extrapolated to the modeling of higher order systems [59].

4.2. Hf-Ta-O System

The CALPHAD models of the Hf-Ta-O system will be described in a separate publication by the authors [9]. Preliminary models result in the phase diagram of the HfO_2-Ta_2O_5 system shown in Fig. 6. Although the phase diagram is consistent with data from prior thermal arrest and in-situ XRPD experiments [11, 48], it requires further optimization in the Thermo-Calc software [57]. Furthermore, the thermodynamic stabilities of the three ternary oxides will be assessed based on the recent calorimetric findings of Voskanyan *et al.* [62].

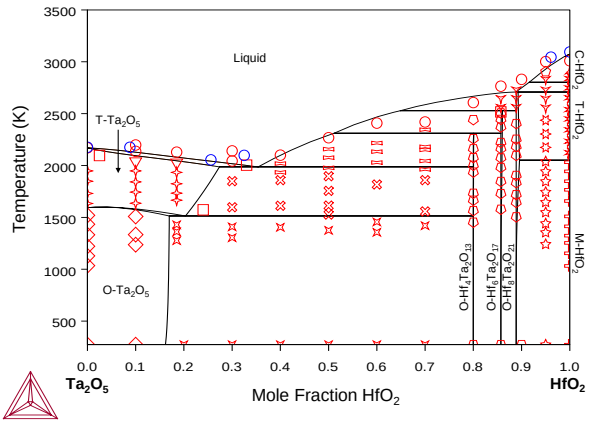

Fig. 6. Preliminary calculated phase diagram of the HfO_2-Ta_2O_5 system between 273.15 and 3500 K. Experimental data from [11] (Red) and [48] (Blue).

5. Conclusions

CALPHAD models of the Ta-O subsystem and preliminary ones of the HfO_2-Ta_2O_5 isopleth were developed using the CEF and ionic liquid model, and generate phase diagrams that agree with experimental data. The Ta-O models favorably estimate the oxygen solubility in BCC Ta and the thermochemical data of both Ta_2O_5 polymorphs, and provide an accurate qualitative prediction of liquid-phase behavior. The liquid phase Ta-O models could be improved with additional liquidus data. First-principles calculations of the formation enthalpies of O-Ta_2O_5 and mixing enthalpies of oxygen in BCC Ta agree with prior experimental data and current models. Regarding CALPHAD modeling of the HfO_2-Ta_2O_5 system, the present Ta-O, revised Hf-O, and prior Hf-Ta assessments were combined with new ternary models. Once optimized, the HfO_2-Ta_2O_5 isopleth will be used to determine the relative stabilities of ternary oxides in the $Hf_{(n-5)/2}Ta_2O_n$ series for optimization of HfC-TaC alloy compositions. Improvement of the oxidation resistance of HfC-TaC alloys will significantly benefit aerospace and space exploration initiatives, and contribute to the study of materials for extreme chemical and thermal conditions. These objectives are consistent with the goals of NASA detailed in its Mission Directorates, as well as those of the Materials Genome Initiative for Global Competitiveness [63-67].

Declaration of Competing Interest

The authors declare that they have no known competing financial interests or personal relationships that could have appeared to influence the work reported in this paper.

Acknowledgements

B.-C.Z. acknowledges support from the University of Virginia start-up funds. R.Z. acknowledges support from the University of Virginia Engineering Distinguished Fellowship and the Virginia Space Grant Consortium (VSGC) Graduate Research Fellowship. Both authors acknowledge support from the Office of Naval Research (ONR) through Grant No. N00014-19-1-2274 by the U.S. Department of Defense. The authors acknowledge Research Computing at the University of Virginia for providing computational resources and technical support that have contributed to the results reported within this publication. URL: https://re.virginia.edu.

References

[1] S. M. Johnson, "Ultra High Temperature Ceramics," National Aeronautics and Space Administration, 2015.
[2] C. Robinson, "Overview of Environmental Durability Coatings and Test Capabilities," Hypersonic Propulsion Materials and Structures Workshop. National Aeronautics and Space Administration, 2019.
[3] J. W. Dankanich and R. L. Frederick, "Marshall Space Flight Center: Research and Technology Report 2020," National Aeronautics and Space Administration, 2020, pp. 64-65.
[4] W. G. Fahrenholtz, "Refractory Diborides of Zirconium and Hafnium," *J. Am. Ceram. Soc.*, vol. 90, no. 5, pp. 1347-1364, 2007.

[5] J. Zhang, S. Wang, W. Li, Y. Yu, and J. Jiang, "Understanding the oxidation behavior of Ta–Hf–C ternary ceramics at high temperature," *Corros. Sci.*, vol. 164, 108348, 2020.
[6] S. J. McCormack and W. M. Kriven, "Crystal structure solution for the $A_6B_2O_{17}$ (A = Zr, Hf; B = Nb, Ta) superstructure," *Acta Crystallogr. B*, vol. 75, pp. 227-234, 2019.
[7] N. Saunders and A. P. Miodownik, *CALPHAD (Calculation of Phase Diagrams): A Comprehensive Guide*, 1 ed.: Pergamon, 1998.
[8] K. J. Meisner, R. Zaman, and B.-C. Zhou, "Thermodynamic modeling of the Ta-O system," *Calphad*, vol. 76, 102391, 2022.
[9] R. Zaman and B.-C. Zhou, "Thermodynamic Modeling of the Hf-Ta-O System for Oxidation Resistance in HfC-TaC Alloys," Manuscript in Preparation.
[10] F. M. Spiridonov, M. N. Mulenkova, V. I. Tsirel'nikov, and L. N. Komissarova, "Intermediate Phases in the HfO_2-Ta_2O_5 System," *Russ. J. Inorg. Chem.*, vol. 26, no. 6, pp. 922-923, 1981.
[11] S. J. McCormack, K.-P. Tseng, R. J. K. Weber, D. Kapush, S. V. Ushakov, A. Navrotsky, and W. M. Kriven, "In-situ determination of the HfO_2–Ta_2O_5-temperature phase diagram up to 3000°C," *J. Am. Ceram. Soc.*, vol. 102, no. 8, pp. 4848-4861, 2018.
[12] P. A. Romans, O. G. Paasche, and H. Kato, "The transformation temperature of hafnium," *J. Less-Common Met.*, vol. 8, no. 3, pp. 213-215, 1965.
[13] M. H. Mueller, "The Lattice Parameter of Tantalum," *Scripta Metall.*, vol. 11, no. 8, pp. 693, 1977.
[14] S. Pathak, P. Das, T. Das, G. Mandal, B. Joseph, M. Sahu, S. D. Kaushik, and V. Siruguri, "Crystal structure of monoclinic hafnia (HfO_2) revisited with synchrotron X-ray, neutron diffraction and first-principles calculations," *Acta Crystallogr. C*, vol. C76, pp. 1034-1042, 2020.
[15] T. Tobase, A. Yoshiasa, H. Arima, K. Sugiyama, O. Ohtaka, T. Nakatani, K.-i. Funakoshi, and S. Kohara, "Pre-Transitional Behavior in Tetragonal to Cubic Phase Transition in HfO_2 Revealed by High Temperature Diffraction Experiments," *Phys. Status Solidi B*, vol. 255, no. 11, 1800090, 2018.
[16] H.-U. Hummel, R. Fackler, and P. Remmert, "Tantaloxide durch Gasphasenhydrolyse, Druckhydrolyse und Transportreaktion aus 2H-TaS_2,: Synthesen von TT-Ta_2O_5 und T-Ta_2O_5 und Kristallstruktur von T-Ta_2O_5 (in German)," *Chem. Ber.*, vol. 125, pp. 551-556, 1992.
[17] X. Q. Liu, X. D. Han, Z. Zhang, L. F. Ji, and Y. J. Jiang, "The crystal structure of high temperature phase Ta_2O_5," *Acta Mater.*, vol. 55, no. 7, pp. 2385-2396, 2007.
[18] N. H. Krikorian and T. C. Wallace, "The Effect of Oxygen and Nitrogen on the Hafnium α-β Transition," *J. Electrochem. Soc.*, vol. 111, no. 12, pp. 1431-1433, 1964.
[19] J. P. Pemsler, "Thermodynamics of the Interaction of Niobium and Tantalum with Oxygen and Nitrogen at Temperatures near the Melting Point," *J. Electrochem. Soc.*, vol. 108, no. 8, pp. 744-750, 1961.
[20] S. P. Garg, N. Krishnamurthy, A. Awasthi, and M. Venkatraman, "The O-Ta (Oxygen-Tantalum) System," *J. Phase Equilib.*, vol. 17, no. 1, pp. 63-77, 1996.
[21] A. I. Zaslavskii, R. A. Zvinchuk, and A. G. Tutov, "X-ray studies on the polymorphism of Ta_2O_5 (In Russian)," *Dokl. Akad. Nauk SSSR*, vol. 104, no. 3, pp. 409-411, 1955.
[22] K. Lehovec, "Lattice Structure of β-Ta_2O_5," *J. Less-Common Met.*, vol. 7, no. 6, pp. 397-410, 1964.
[23] N. Terao, "Structure des Oxides de Tantale (In French)," *Jpn. J. Appl. Phys.*, vol. 6, no. 1, pp. 21-34, 1967.
[24] A. Fukumoto and K. Miwa, "Prediction of hexagonal Ta_2O_5 structure by first-principles calculations," *Phys. Rev. B*, vol. 55, no. 17, pp. 11155-11160, 1997.
[25] G. M. Wolten and A. B. Chase, "Single-crystal data for β Ta_2O_5 and *A* KPO_3," *Z. Kristallogr.*, vol. 129, pp. 365-368, 1969.
[26] N. C. Stephenson and R. S. Roth, "Structural Systematics in the Binary System Ta_2O_5-WO_3. V. The Structure of the Low-Temperature Form of Tantalum Oxide *L*-Ta_2O_5," *Acta Crystallogr. B*, vol. 27, pp. 1037-1044, 1971.
[27] I. P. Zibrov, V. P. Filonenko, M. Sundberg, and P.-E. Werner, "Structures and phase transitions of *B*-Ta_2O_5 and *Z*-Ta_2O_5: two high-pressure forms of Ta_2O_5," *Acta Crystallogr. B*, vol. 56, no. 4, pp. 659-665, 2000.
[28] L. A. Aleshina and S. V. Loginova, "Rietveld analysis of X-ray diffraction pattern from β-Ta_2O_5 oxide," *Crystallogr. Rep.*, vol. 47, no. 3, pp. 460-464, 2002.
[29] I. E. Grey, W. G. Mumme, and R. S. Roth, "The crystal chemistry of L-Ta_2O_5 and related structures," *J. Solid State Chem.*, vol. 178, no. 11, pp. 3308-3314, 2005.
[30] H. Sawada and K. Kawakami, "Electronic structure of oxygen vacancy in Ta_2O_5," *J. Appl. Phys.*, vol. 86, no. 2, pp. 956-959, 1999.
[31] J.-H. Yuan, K.-H. Xue, Q. Chen, L. R. C. Fonseca, and X.-S. Miao, "Ab Initio Simulation of Ta_2O_5: A High Symmetry Ground State Phase with Application to Interface Calculation," *Ann. Phys. (Berlin)*, vol. 531, no. 8, 1800524, 2019.
[32] R. Ramprasad, "First principles study of oxygen vacancy defects in tantalum pentoxide," *J. Appl. Phys.*, vol. 94, no. 9, pp. 5609-5612, 2003.
[33] S.-H. Lee, J. Kim, S.-J. Kim, S. Kim, and G.-S. Park, "Hidden Structural Order in Orthorhombic Ta_2O_5," *Phys. Rev. Lett.*, vol. 110, no. 23, 235502, 2013.
[34] A. Jain, S. P. Ong, G. Hautier, W. Chen, W. D. Richards, S. Dacek, S. Cholia, D. Gunter, D. Skinner, G. Ceder, and K. A. Persson, "Commentary: The Materials Project: A materials genome approach to accelerating materials innovation," *APL Mater.*, vol. 1, no. 1, 011002, 2013.
[35] J.-Y. Kim, B. Magyari-Köpe, K.-J. Lee, H.-S. Kim, S.-H. Lee, and Y. Nishi, "Electronic structure and stability of low symmetry Ta_2O_5 polymorphs," *Phys. Status Solidi RRL*, vol. 8, no. 6, pp. 560-565, 2014.
[36] E. Gebhardt and H. Seghezzi, "Investigations in the tantalum-oxygen system II. Reactions and equilibria

between mixed crystals and oxide phases (In German)," *Z. Metallkd.,* vol. 50, pp. 248-257, 1959.
[37] H. Jehn and E. Olzi, "High temperature solid-solubility limit and phase studies in the system tantalum-oxygen," *J. Less-Common Met.,* vol. 27, no. 3, pp. 297-309, 1972.
[38] W. Nickerson and C. Altstetter, "Thermodynamic properties of tantalum-oxygen solid solutions," *Scripta Metall.,* vol. 7, no. 4, pp. 377-382, 1973.
[39] J. S. Lee and C. J. Altstetter, "Thermodynamic studies of oxygen behavior in tantalum-based alloys," *Acta Metall.,* vol. 34, no. 1, pp. 139-145, 1986.
[40] H. S. Hong and K. S. Lee, "Thermodynamic evaluation of the Ta–O system from pure tantalum to tantalum pentoxide," *J. Alloy. Compd.,* vol. 360, no. 1-2, pp. 198-204, 2003.
[41] E. Fromm and R. Kirchheim, "EMF-measurements in oxygen–VA metals systems using a ThO_2–Y_2O_3 solid electrolyte (In German)," *Z. Metallkd.,* vol. 66, no. 3, pp. 144-150, 1975.
[42] K. T. Jacob, C. Shekhar, and Y. Waseda, "An update on the thermodynamics of Ta_2O_5," *J. Chem. Thermodyn.,* vol. 41, no. 6, pp. 748-753, 2009.
[43] D. Shin, R. Arróyave, and Z.-K. Liu, "Thermodynamic modeling of the Hf–Si–O system," *Calphad,* vol. 30, no. 4, pp. 375-386, 2006.
[44] D. Shin, "Thermodynamic Properties of Solid Solutions from Special Quasirandom Structures and CALPHAD Modeling: Application to Al-Cu-Mg-Si and Hf-Si-O," Department of Materials Science and Engineering, The Pennsylvania State University, 2007.
[45] C. Wang, "Experimental and Computational Phase Studies of the ZrO_2-based Systems for Thermal Barrier Coatings," Department of Chemistry, Max-Planck-Institut für Metallforschung, Stuttgart, 2006.
[46] A. F. Guillermet, "Gibbs Energy Modelling of the Phase Diagram and Thermochemical Properties in the Hf-Ta System," *Z. Metallkd.,* vol. 86, no. 6, pp. 382-387, 1995.
[47] S. J. McCormack, K.-P. Tseng, R. J. K. Weber, D. Kapush, S. V. Ushakov, A. Navrotsky, and W. M. Kriven, "Reply to comments: "In-situ determination of the HfO_2-Ta_2O_5-temperature phase diagram up to 3000°C"," *J. Am. Ceram. Soc.,* vol. 102, no. 11, pp. 7028-7030, 2019.
[48] R. P. Turcotte, *Phase Relationships in High Temperature Ceramics*, Naval Surface Weapons Center, Silver Spring, Maryland, 1987.
[49] D. M. Ceperley and B. J. Alder, "Ground State of the Electron Gas by a Stochastic Method," *Phys. Rev. Lett.,* vol. 45, no. 7, pp. 566-569, 1980.
[50] A. van de Walle, P. Tiwary, M. de Jong, D. L. Olmsted, M. Asta, A. Dick, D. Shin, Y. Wang, L.-Q. Chen, and Z.-K. Liu, "Efficient stochastic generation of special quasirandom structures," *Calphad,* vol. 42, pp. 13-18, 2013.
[51] A. van de Walle, Q. Hong, S. Kadkhodaei, and R. Sun, "The free energy of mechanically unstable phases," *Nat. Commun.,* vol. 6, 7559, 2015.
[52] H. Lukas, S. Fries, and B. Sundman, *Computational Thermodynamics*, New York: Cambridge University Press, 2007.
[53] B. Sundman and J. Ågren, "A Regular Solution Model for Phases with Several Components and Sublattices, Suitable for Computer Applications," *J. Phys. Chem. Solids,* vol. 42, no. 4, pp. 297-301, 1981.
[54] H. Harvig, "An Extended Version of the Regular Solution Model for Stoichiometric Phases and Ionic Melts," *Acta Chem. Scand.,* vol. 25, pp. 3199-3204, 1971.
[55] O. Redlich and A. T. Kister, "Algebraic Representation of Thermodynamic Properties and the Classification of Solutions," *Ind. Eng. Chem.,* vol. 40, no. 2, pp. 345-348, 1948.
[56] A. T. Dinsdale, "SGTE data for pure elements," *Calphad,* vol. 15, no. 4, pp. 317-425, 1991.
[57] J.-O. Andersson, T. Helander, L. Höglund, P. Shi, and B. Sundman, "Thermo-Calc & DICTRA, computational tools for materials science," *Calphad,* vol. 26, no. 2, pp. 273-312, 2002.
[58] M. Cancarevic, M. Zinkevich, and F. Aldinger, "Thermodynamic description of the Ti–O system using the associate model for the liquid phase," *Calphad,* vol. 31, no. 3, pp. 330-342, 2007.
[59] M. Hillert, B. Jansson, B. Sundman, and J. Ågren, "A Two-Sublattice Model for Molten Solutions with Different Tendency for Ionization," *Metall. Trans. A,* vol. 16A, pp. 261-266, 1985.
[60] S. Lagergren and A. Magnéli, "On the Tantalum - Oxygen System," *Acta Chem. Scand.,* vol. 6, pp. 444-446, 1952.
[61] A. Reisman, F. Holtzberg, M. Berkenblit, and M. Berry, "Reactions of the Group VB Pentoxides with Alkali Oxides and Carbonates. III. Thermal and X-Ray Phase Diagrams of the System K_2O or K_2CO_3 with Ta_2O_5," *J. Am. Chem. Soc.,* vol. 78, no. 18, pp. 4514–4520, 1956.
[62] A. A. Voskanyan, K. Lilova, S. J. McCormack, W. M. Kriven, and A. Navrotsky, "A new class of entropy stabilized oxides: Commensurately modulated $A_6B_2O_{17}$ (A = Zr, Hf; B = Nb, Ta) structures," *Scripta Mater.,* vol. 204, 114139, 2021.
[63] T. Kalil and C. Wadia, *Materials Genome Initiative for Global Competitiveness*, National Science and Technology Council, ed., 2011.
[64] R. Pearce, "NASA Aeronautics Strategic Implementation Plan 2019 Update," National Aeronautics and Space Administration, 2019.
[65] K. Lueders, "About the Human Exploration and Operations Mission Directorate," National Aeronautics and Space Administration, 2021.
[66] T. Zurbuchen, "SCIENCE 2020-2024: A Vision for Scientific Excellence," National Aeronautics and Space Administration, 2020.
[67] C. Bolden, "NASA Strategic Space Technology Investment Plan," National Aeronautics and Space Administration, 2012.